

THE IMPACT OF THE SPECTRAL RESPONSE OF AN ACHROMATIC HALF-WAVE PLATE ON THE MEASUREMENT OF THE COSMIC MICROWAVE BACKGROUND POLARIZATION

C.BAO¹, B.GOLD¹, C.BACCIGALUPI², J.DIDIER³, S.HANANY¹, A.JAFFE⁴, B.R.JOHNSON³, S.LEACH², T.MATSUMURA⁵,
A.MILLER³ AND D.O'DEA⁴

Draft version November 5, 2018

ABSTRACT

We study the impact of the spectral dependence of the linear polarization rotation induced by an achromatic half-wave plate on measurements of cosmic microwave background polarization in the presence of astrophysical foregrounds. We focus on the systematic effects induced on the measurement of inflationary gravitational waves by uncertainties in the polarization and spectral index of Galactic dust. We find that for the experimental configuration and noise levels of the balloon-borne EBEX experiment, which has three frequency bands centered at 150, 250, and 410 GHz, a crude dust subtraction process mitigates systematic effects to below detectable levels for 10% polarized dust and tensor to scalar ratio of as low as $r = 0.01$. We also study the impact of uncertainties in the spectral response of the instrument. With a top-hat model of the spectral response for each band, characterized by band-center and band-width, and with the same crude dust subtraction process, we find that these parameters need to be determined to within 1 and 0.8 GHz at 150 GHz; 9 and 2.0 GHz at 250 GHz; and 20 and 14 GHz at 410 GHz, respectively. The approach presented in this paper is applicable to other optical elements that exhibit polarization rotation as a function of frequency.

Subject headings: cosmic microwave background — instrumentation: polarimeters — methods: data analysis

1. INTRODUCTION

The Cosmic Microwave Background (CMB) polarization field can be decomposed into two orthogonal E and B modes. On large angular scales the B-mode signal encodes information about inflation, a period of rapid expansion in the early universe (Kamionkowski et al. 1997; Seljak & Zaldarriaga 1997). The signal is characterized by the tensor-to-scalar ratio r which quantifies the relative strength of inflationary gravitational waves (IGW) and density perturbations generated by inflation. The level of the IGW signal encodes information about the energy scale at which inflation occurred. The current upper limit is $r < 0.2$ (Komatsu et al. 2011). A number of experimental efforts are ongoing to search for the signal at levels as low as $r \sim 0.01$ over the coming years. On small angular scales, the B-mode signal is dominated by the ‘lensing signal’, which results from gravitational lensing of the CMB photons by the large scale structure of the universe. The lensing converts E-mode to B-mode polarization (Zaldarriaga & Seljak 1998).

Galactic foregrounds are expected to be a source of confusion for measurements of the B-mode signal. Above 70 GHz the polarized emission from Galactic dust is predicted to dominate over much of the sky and be comparable to the IGW signal with an r value of 0.1 or less even for the cleanest regions of the sky (Page et al. 2007; Gold et al. 2009; Fraisse et al. 2011). Therefore many

experimental efforts plan to employ multiple frequencies which will enable foreground identification and subtraction.

Some CMB polarimeters use a half-wave plate (HWP) to modulate the observed linear polarization, such as EBEX (Reichborn-Kjennerud et al. 2010), SPIDER (Runyan et al. 2010) and POLARBEAR (Arnold et al. 2010). When observing at multiple frequency bands simultaneously, an achromatic half-wave plate (AHWP) can be used. An AHWP is a stack of monochromatic HWPs with a particular set of orientation angles relative to each other (Pancharatnam 1955). While an AHWP has a higher modulation efficiency across a broad frequency range compared to a single HWP, it rotates the polarization angle of the incident light by an amount that depends on frequency (Hanany et al. 2005; Matsumura et al. 2009). The amount of rotation depends on the construction parameters of the AHWP and on the spectrum and polarized intensity of the constituent signals, which for this paper are CMB and Galactic dust. With knowledge of the spectrum and relative polarization intensity, the amount of rotation can be calculated and corrected. However, while the spectrum of the CMB component is well known, that of dust is not. The polarized intensities of dust and CMB are also not well known. These uncertainties may pose challenges in the extraction of the underlying IGW signal. Various authors studied the impact of HWP non-idealities on measurements of CMB polarization (Brown et al. 2009; Bryan et al. 2010). However, this particular frequency dependent rotation effect has not been studied in the context of B-mode measurements. The goal of this paper is to quantitatively assess this effect. For concreteness we adopt the AHWP model, frequency bands and approximate noise information that are applicable to the E

¹ University of Minnesota School of Physics and Astronomy, Minneapolis, MN 55455

² SISSA, Astrophysics Sector, via Bonomea 265, Trieste 34136, Italy

³ Columbia University, New York, NY 10027

⁴ Imperial College, London, SW72AZ, England, United Kingdom

⁵ High Energy Accelerator Research Organization (KEK), 1-1 Oho, Tsukuba, Ibaraki 305-0801, Japan

and B experiment (EBEX) (Reichborn-Kjennerud et al. 2010), a balloon-borne CMB polarimeter targeting the IGW signal at the $r \sim 0.04$ level.

In Section 2 we describe the basic components of the simulation. Section 3 focuses on quantifying the effect of rotation due to the AHWP in the 150 GHz band. In Section 4 we use multiple frequency information to account for rotation due to Galactic dust. In Section 5, we study the additional effects of uncertainties in the spectral response of the instrument, and in Section 6 we make concluding remarks.

2. DESCRIPTION OF THE SIMULATION

We simulate input Stokes Q and U signals due to the CMB and Galactic dust emission on a $10^\circ \times 10^\circ$ area of the sky centered on $(l, b) = (252^\circ, -52^\circ)$ in Galactic coordinates which is close to the center of the area targeted by EBEX. The maps are smoothed with an $8'$ FWHM Gaussian beam then projected to a flat sky and pixelized with a square $6.9'$ pixel. Same simulations with a $20^\circ \times 20^\circ$ patch in the same region validate that conclusions presented in this paper do not depend on patch size. The input CMB polarization angular power spectra, including both the primordial and lensing signal, are generated with CAMB (Lewis et al. 2000) using the best fit WMAP 7-year cosmological parameters (Komatsu et al. 2011) and $r = 0.05$, unless otherwise indicated. Our polarized foreground simulation follows the prescription detailed in Stivoli et al. (2010) and is briefly reviewed here. The dust intensity and its frequency scaling are given by ‘model 8’ of Finkbeiner et al. (1999). The dust polarization fraction is modeled for cases of 2%, 5%, and 10%. A polarization fraction higher than 10% would exceed the limit based on WMAP observations at intermediate and high Galactic latitudes (Page et al. 2007; Gold et al. 2009). Both the dust polarization fraction and the frequency scaling are assumed to be uniform over the simulated sky area. Observations suggest that this is a good approximation (Planck Collaboration et al. 2011; Finkbeiner et al. 1999). The pattern of the polarization angles on large angular scales ($l \lesssim 100$) is given by the WMAP dust polarization template (Page et al. 2007). On smaller angular scales ($l \gtrsim 100$) we add a Gaussian fluctuation power adopting a recipe first presented by Giardino et al. (2002). Figure 1 shows the power spectra of the CMB and of Galactic dust. For a level of 5% fractional polarization the expected level of Galactic dust is comparable to the B-mode signal at $l = 90$.

To simulate the operation of the AHWP we use the Mueller matrix formalism as described by Matsumura et al. (2009). The level of input polarized signal is calculated for each map pixel in 50 frequency bins for each of the experiment’s three top-hat bands (see Table 1). For each map pixel the detected intensity as a function of AHWP angle, which we call intensity vs. angle (IVA), is calculated for each frequency bin with an angular resolution of 0.05° and the total per-band IVA is the average of the 50 IVAs. The detected polarization angle, which is rotated relative to the input polarization angle, is encoded by the phase of the band-averaged IVA. To obtain the rotated map observed by the detector, we multiply each pixel of the input maps by a rotation matrix with the calculated phase of the band-averaged IVA. The frequency and IVA angular resolution are chosen to

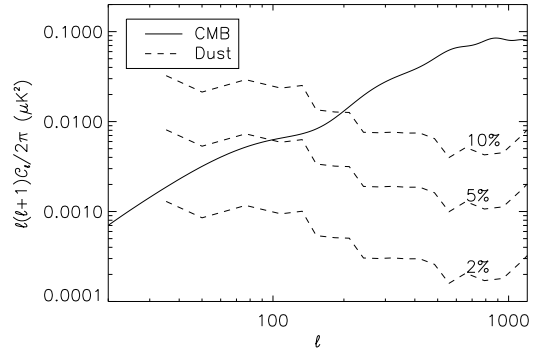


FIG. 1.— CMB (solid) and Galactic dust (dashed) B-mode power spectra at 150 GHz assuming an r value of 0.05. The spectra from dust are for the specific area of sky simulated in this work and are given for three fractional polarization cases of 2, 5, and 10 %.

optimize computation time while giving negligible bias in the results. The construction parameters of the AHWP are given in Table 1.

Indices of refraction of AHWP	$n_o = 3.047, n_e = 3.364$
Thickness of each wave plate	1.69 mm
150 GHz band	133 - 173 GHz
250 GHz band	217 - 288 GHz
410 GHz band	366 - 450 GHz
Band shape	top-hat
Orientation angles of 5-stack AHWP	$(0^\circ, 25^\circ, 88.5^\circ, 25^\circ, 0^\circ)$

TABLE 1
AHWP AND BAND PARAMETERS USED IN THE SIMULATIONS.

We calculate both EE and BB power spectra simultaneously using the flat-sky approximation (Kaiser 1992). Each simulation is run 100 times with different CMB and noise realization, unless otherwise noted. In this study we focus on the BB power spectra. The result quoted for a given l bin is the mean of the 100 simulations and the error bar is the standard deviation. Figure 2 shows a validation of the process of generating CMB Q and U maps and estimating the underlying E and B-mode power spectra. No rotation due to the AHWP has been included in this validation.

For simulations that include the effects of instrumental noise we assume it is homogeneous and has a white spectrum, and add its realization to the signal to make a combined input map. In our simulation we use an instrumental noise per pixel of 1, 2.8, and $25 \mu\text{K}_{\text{CMB}}$ for the 150, 250, and 410 GHz bands, respectively. Figure 2 shows a validation of the noise generation and estimation process.

3. THE EFFECT OF GALACTIC DUST

If the shape of the frequency band is known then the rotation induced on the CMB signal alone can be calculated and compensated exactly because the spectrum of the CMB is known. This rotation is uniform across the sky and with the parameters given in Table 1 is 55° in the 150 GHz band. The presence of Galactic dust modifies the intensity and angle of the net incident polarization and thus the amount of rotation induced by the

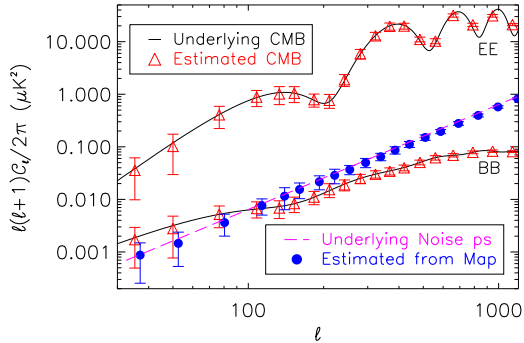


FIG. 2.— Validation of signal and noise power spectrum estimation. We generate 100 Q and U maps using an underlying power spectra (black solid curves) and use a flat-sky approximation to estimate the power spectra (red triangles with error bars). The size of error bars agrees with predictions for the contributions of cosmic and sample variance. We also make 100 noise only Q and U realizations using white noise with RMS of $1 \mu\text{K}$ (magenta dashed line) and estimate the power spectrum (blue solid circles with error bars). The estimated noise power spectrum is shown slightly offset in ℓ to enhance clarity.

AHWP. The spectral dependence and spatial distribution of Galactic dust polarization is not precisely known and therefore the amount of rotation it induces can only be estimated. How big is this extra rotation? Can it simply be ignored because it is negligible? In the remainder of this section we assess these questions for the 150 GHz band.

These first simulations include CMB and dust, without instrumental noise. We calculate rotated Q and U maps resulting from passing the total (CMB+dust) incoming polarization through the AHWP. We then ‘de-rotate’ the maps by the calculated rotation angle for CMB only, simulating ignorance of the effects of the dust foreground on the rotation. We subtract the input dust Q and U maps from the de-rotated map to acknowledge the presence of the effects of dust *polarized intensity* on the total Q and U maps. Note however that the effect of *rotation due to dust polarization*, which is a consequence of the AHWP, is left in the map. We then calculate the angular power spectrum of the resulting maps for 2%, 5%, and 10% of dust polarization (see Figure 3). For the fiducial value of $r = 0.05$ ignoring the effect of rotation introduces noticeable bias in the estimation of the CMB power spectrum for 10% dust polarization but not for 2% dust polarization. For 5% dust polarization the bias is only noticeable in the lowest two and the highest ℓ bins.

4. REMOVING AHWP INDUCED ROTATION IN DUST SUBTRACTION

In the previous section we showed that for levels of polarized dust of more than 5% the effect of the rotation due to dust in the AHWP cannot be ignored. In this section we employ a simple form of dust subtraction in an attempt to correct for the rotation. In this approach we make two initial assumptions in order to extract the dust frequency scaling information:

1. the signal at the 150 GHz band is dominated by the CMB and dust can be neglected;
2. the signal at the 410 GHz band comes entirely from

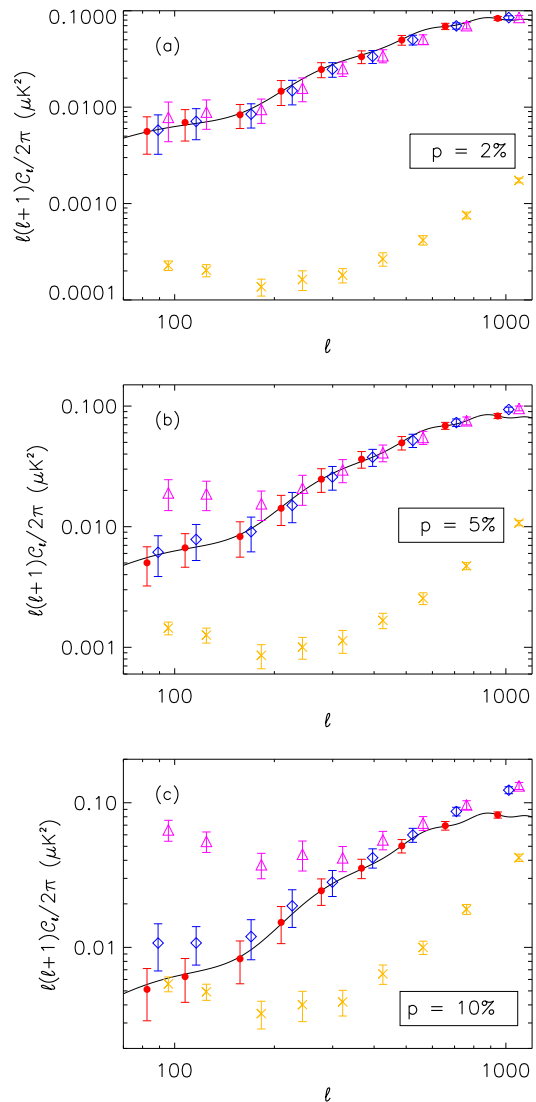


FIG. 3.— Effect of rotation due to 2%, 5%, and 10% polarized dust on the estimation of the B-mode power spectrum. The input CMB power spectrum (red solid circles) follows the underlying assumed power spectrum (black solid line). The difference between the input CMB and the power spectrum of the map after de-rotation by the rotation angle corresponding to the CMB alone (magenta triangles) indicates the effect of polarized dust. After subtracting the dust intensity, only the *rotation* due to the presence of dust remains (blue diamonds). The power spectrum of a map of the difference between the input map and the de-rotated, dust-subtracted map (yellow crosses) quantifies the effect of the rotation due to dust alone. Power spectra points are all calculated at the same ℓ bins but are shown slightly offset in ℓ to enhance clarity. To reduce clutter we only plot data for every other ℓ bin for $\ell > 120$.

dust and CMB can be neglected;

We prepare the total (CMB+dust) rotated polarization maps in 150, 250, and 410 GHz bands and add noise in the map domain. We then calculate the polarization intensity maps and the signal RMS in all three bands assuming that the noise RMS is exactly known. Following assumption 1 the map RMS of CMB at 150 GHz is known. We extrapolate the CMB level to 250 GHz and calculate the map RMS for dust at 250 GHz. Following

assumption 2 we also obtain the map RMS for dust at 410 GHz. Using the dust levels at 250 and 410 GHz we fit a gray body dust model, given by a power law multiplied by an 18 K blackbody. The power law spectral index is taken to be uniform across the entire simulated sky area. The top hat spectral response of the instrument is assumed to be precisely known (we address uncertainties in the bandpass in Section 5). The fitted dust model is used to calculate the level of dust at the 150 GHz band, extrapolated from the 410 GHz map, and to calculate and correct for the rotation angle at this band due to the combination of dust and CMB. We make a final map that contains an estimate of the CMB alone after corrections for both dust polarized intensity and rotation induced by the AHWP. We calculate the power spectrum of this map including subtraction of an estimate of the noise spectrum. For an estimate of the noise spectrum we use the known input RMS. As a test of the entire pipeline we run it with no dust and no noise and validate that the extracted power spectrum agrees with the input CMB power spectrum.

For each set of 100 simulations, we determine whether the final estimated CMB power spectrum is biased or not. The power spectrum is conservatively assumed biased if the mean power estimated in *any* ℓ bin is outside of the $1\text{-}\sigma$ cosmic variance error bar. We find that for the nominal noise levels, $r = 0.01$ or above, and all dust polarized fractions at or below 10% the dust subtraction procedure recovers an unbiased estimate of the B-mode power spectrum. The results for 10% dust polarization fraction are shown in Figure 4. Only data points with signal to noise ratio (SNR) > 1 are plotted. For $r = 0.009$ and lower, and 10% dust polarization fraction, we find that the recovered B-mode power spectrum is biased at the lowest ℓ bin. When the dust polarization is lower the r level that can be recovered without bias is higher because the higher relative noise at 410 GHz has a larger effect on the CMB estimate at 150 GHz. For 2% dust polarization fraction, we can recover r as low as 0.02.

We also use a different approach to quantify the bias caused by the dust subtraction procedure. We run 100 simulations with an input of $r = 0$ and 10% dust polarization fraction. We fit a non-zero r to the difference between the estimated and input CMB power spectrum at the lowest ℓ bin, while keeping the shape of the primordial B mode signal. We consider this fit as the lower limit of r value we can detect using this dust subtraction method. We find a best fit with $r = 0.01$, which is close to the result we found earlier.

The error bars shown in Figure 4 include only cosmic variance for the input CMB, but include the total error on the recovered CMB power spectrum (including the effect of correcting for the rotation). On average the total error is larger by 30% compared to the error from the combination of cosmic variance and instrument noise (Fig. 4, upper panel).

5. UNCERTAINTY IN DETECTION BAND AND HIGH FREQUENCY SPECTRAL RESPONSE

So far we assumed that the spectral response of the instrument is known. Only the frequency scaling of Galactic dust is determined from the fit. Uncertainty in the spectral response leads to uncertainty in the amount of rotation induced by the AHWP. To assess the level

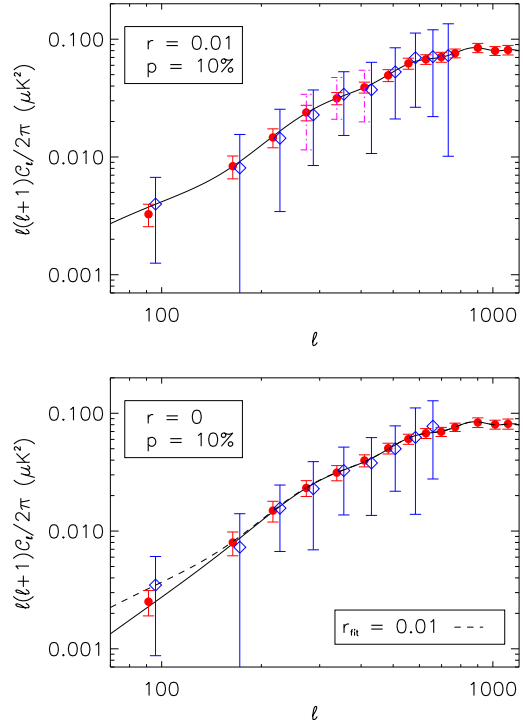


FIG. 4.— Comparison between the underlying CMB model (black line), the input CMB (red circles, error bars include only cosmic variance) and the estimate of the CMB power spectrum using a map in which the effects of both dust polarized intensity and dust induced extra rotation has been accounted for (blue diamonds). The final error bars are on average 30% larger than those due to cosmic variance *and* instrument noise (magenta dot-dashed error bars, only plotted in three mid- ℓ range bins for clarity). With 10% dust polarization, a crude dust subtraction algorithm (see text) can account for the rotation induced in the AHWP with an r value as low as 0.01 (top panel). In the bottom panel the input r is zero and the underlying CMB spectrum has only a lensing signal; Galactic dust is 10% polarized. The estimated CMB spectrum has a best fit $r = 0.01$. To reduce clutter we only plot data at every other ℓ bin for $\ell > 800$.

of this effect quantitatively we assume a top-hat band shape that is characterized by two parameters, center and width. We simulate CMB and dust signals with *nominal* bands, and analyze the maps using the dust subtraction algorithm discussed in the previous section but assuming varying band-widths, or varying band-centers (but not both simultaneously). No instrumental noise is included. All simulations have 10% polarized dust and $r = 0.05$. We search for the level of shift in band-center or change in width that leads to bias in the estimation of the final CMB spectrum. We use the same criterion for bias as described in Section 4.

5.1. Shift of Band-Center

Simulations are carried out by shifting only one band-center, keeping the other two fixed at their nominal values. We find that shifts of more than 1, 9, and 20 GHz for the 150, 250, and 410 GHz bands, respectively, lead to biased power spectra. The limit for shift of the 150 GHz band is due to mixing between E and B modes: an error in band-center leaves the CMB slightly rotated after correction for the AHWP is applied (using the nominal band) and thus a portion of the E-mode signal is mixed

into the B-mode signal. This is apparent in Figure 5 (panel b), which shows a 2 GHz shift for the 150 GHz; the bias is primarily at high ℓ . The limits on the 250 and 410 GHz bands mainly come from misestimate of rotation due to dust, but because dust is not dominant at the 150 GHz band the requirement is less stringent. Panels (c) and (d) in Figure 5 show shifts of 10 and 22 GHz for the 250 and 410 GHz bands, in which bias due to dust is found only at the lowest ℓ bin.

5.2. Misestimate of Band-Width

Simulations are carried out by changing one bandwidth at a time, keeping the other two fixed at their nominal values. We find that a misestimate of bandwidth by more than 0.8, 2, or 14 GHz for the 150, 250, and 410 GHz band, respectively, exceeds the criterion for no bias. The result for the 150 GHz band with a change of 1 GHz in width is shown in Figure 6. The cause of bias in any of the bands is a misestimate of total power detected at the particular band thus a misestimate of both the polarized signal intensity and the rotation due to dust. For this reason the bias is largest at the lowest ℓ bins.

5.3. Effects of High Frequency Spectral Leak

Dust intensity is rising up to ~ 2 THz. A higher than expected and unknown instrumental response at out-of-band frequencies, which is called a ‘spectral leak’, may bias the subtraction of the dust signal and by extension the estimate of the underlying CMB signal. We simulate two specific leaks, which are both top-hat in shape, a narrow leak between 1750 and 1850 GHz and a broad leak between 500 and 2000 GHz. For both cases the power in the leak is adjusted to be 0.1%, 1% and 1% of the in-band power for the 150, 250, and 410 GHz bands, respectively, as measured with a 300 K black-body source. These values are readily achievable experimentally (Polsgrove 2009). We properly include the change in the refraction indices of sapphire with frequency (Loewenstein et al. 1973). Maps are prepared with signals that include power in the leak, but are analyzed, including the steps of dust subtraction, assuming no knowledge of the leak. Instrumental noise is not included in the simulation. For both cases we find no biases in the estimate of the final CMB power spectrum. Figure 7 shows the case for the broad leak.

6. DISCUSSION AND SUMMARY

The spectral response of an achromatic half-wave plate may induce bias in the estimation of polarized signals. We analyze the level of such bias in the context of measurements of the B-mode signal of the CMB in the presence of Galactic dust, the dominant source of foreground emission in cases of interest here. For concreteness, we use the specific experimental configuration corresponding to the EBEX balloon-borne experiment.

For the area of sky considered we find that with reasonable assumptions about the magnitude and spectral shape of dust, the effects of rotation induced by the AHWP are only appreciable when dust is polarized at a level of about 5% and above and the tensor-to-scalar ratio r is less than ~ 0.05 . In the regime when the effects of rotation are appreciable, even a crude process of

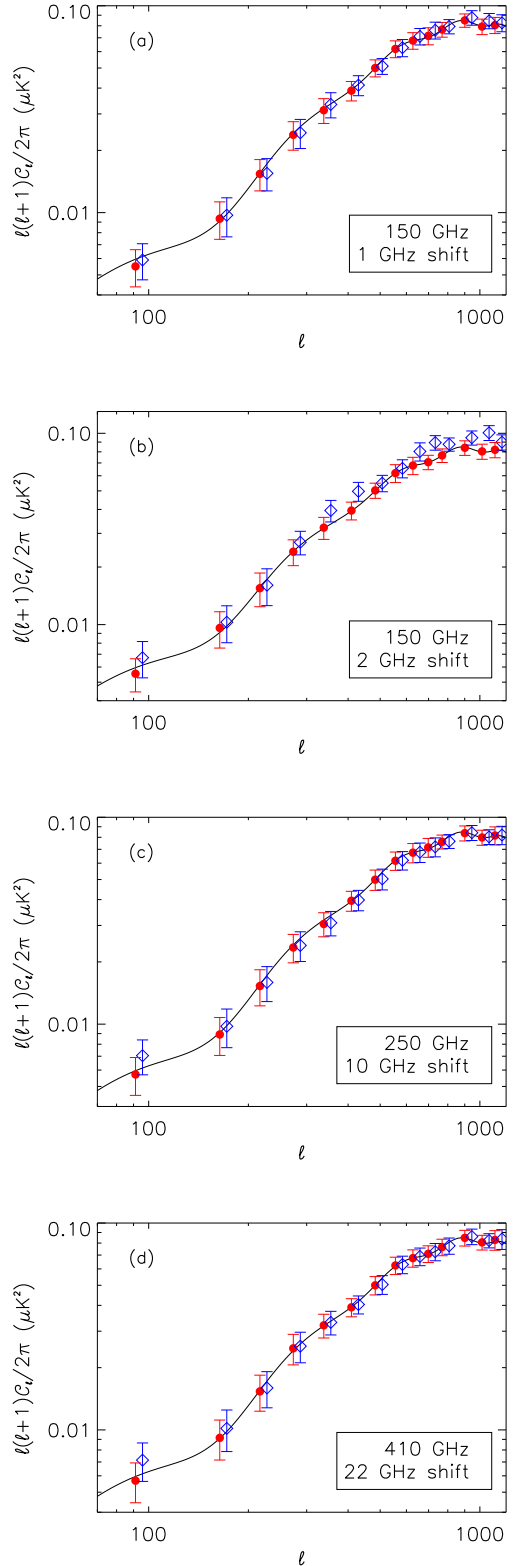


FIG. 5.— Effect of band-center shift of 1 GHz of the 150 GHz band (panel a), 2 GHz of the 150 GHz band (panel b), 10 GHz of the 250 GHz band (panel c) and 22 GHz of the 410 GHz band (panel d), respectively. In panel (b) excess power at high ℓ comes from mixing of E and B-mode. In panels (c) and (d) it comes from misestimate of the effects of dust. Figure symbols are the same as in Figure 4.

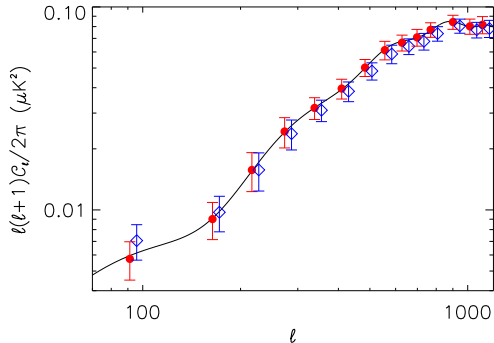


FIG. 6.— A 1 GHz increase in the assumed band-width of the 150 GHz band relative to the nominal width leads to an overestimate of the level of dust in this band and thus to a misestimate of the rotation due to dust. This leads to excess power at low ℓ . The misestimate of the band-width also results in an underestimate of the CMB power which leads to a small (less than $1\text{-}\sigma$) power deficit at high ℓ bins. Figure symbols are the same as in Figure 4.

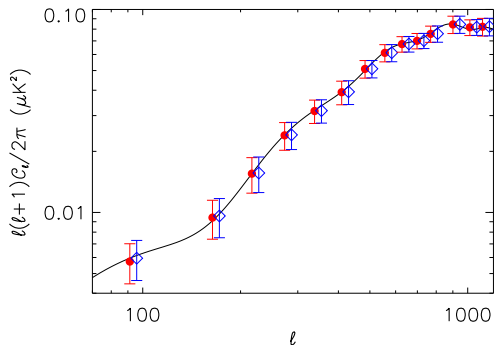


FIG. 7.— The effect of a broad high frequency spectral leak (see text for details) is negligible with $r = 0.05$ and 10% dust polarization. Figure symbols are the same as in Figure 4.

dust estimation and subtraction mitigates the effects of AHWP rotation to below detectable levels. For example, using the crude dust subtraction process we find no

bias in the estimation of the B-mode power spectrum for dust polarization fraction as large as 10% and r as low as 0.01. For 2% dust polarization fraction, r of 0.02 or higher is recovered without bias. We also find that the dust subtraction causes the power spectrum error bars to increase by a modest 30% on average.

Employing the same dust estimation and subtraction process, but now assuming errors in knowledge of the experiment's detection band-center and band-width, we find the accuracy with which these need to be measured. For example, for the particular experimental configuration considered, we found that band-center and band-width of the 150 GHz band need to be determined to better than 1 and 0.8 GHz, respectively. It is possible that this requirement may not need to be as stringent if a more sophisticated foreground estimation and subtraction process is used. This research is ongoing.

We explore the sensitivity of the particular experimental configuration to high frequency spectral leaks. Using a rejection level that is readily achievable experimentally we show that spectral leaks are not expected to pose challenges for the operation with an AHWP.

The analysis and subtraction approach discussed in this paper are applicable to other optical elements for which polarization rotation is a function of frequency. For example, O'Brien (2010) describes a broadband, mm-wave detection technique that is based on sinuous antenna. It is well documented that such antennas change the phase response of polarized signals, and that this effect is frequency dependent. Thus they exhibit fundamentally the same behavior as an AHWP. Our methods and approach apply to such cases.

This research project is supported by a National Science Foundation (NSF) grant 00011640. We are greatly thankful for the computing resources provided by the Minnesota Supercomputing Institute. EBEX is supported through NASA grants NNX08AG40G and NNX07AP36H. C.Baccigalupi and S.Leach acknowledge travel support from the PD51 INFN grant. A.Jaffe acknowledges the support from the STFC in the UK.

REFERENCES

- Arnold, K., et al. 2010, in Society of Photo-Optical Instrumentation Engineers (SPIE) Conference Series, Vol. 7741, Society of Photo-Optical Instrumentation Engineers (SPIE) Conference Series
- Brown, M. L., Challinor, A., North, C. E., Johnson, B. R., O'Dea, D., & Sutton, D. 2009, MNRAS, 397, 634
- Bryan, S. A., Montroy, T. E., & Ruhl, J. E. 2010, Appl. Opt., 49, 6313
- Finkbeiner, D. P., Davis, M., & Schlegel, D. J. 1999, ApJ, 524, 867
- Fraisse, A. A., et al. 2011, ArXiv e-prints, 1106.3087
- Giardino, G., Banday, A. J., Górski, K. M., Bennett, K., Jonas, J. L., & Tauber, J. 2002, A&A, 387, 82
- Gold, B., et al. 2009, ApJS, 180, 265
- Hanany, S., Hubmayr, J., Johnson, B. R., Matsumura, T., Oxley, P., & Thibodeau, M. 2005, Appl. Opt., 44, 4666
- Kaiser, N. 1992, ApJ, 388, 272
- Kamionkowski, M., Kosowsky, A., & Stebbins, A. 1997, Physical Review Letters, 78, 2058
- Komatsu, E., et al. 2011, ApJS, 192, 18
- Lewis, A., Challinor, A., & Lasenby, A. 2000, ApJ, 538, 473
- Loewenstein, E. V., Smith, D. R., & Morgan, R. L. 1973, Appl. Opt., 12, 398
- Matsumura, T., Hanany, S., Ade, P., Johnson, B. R., Jones, T. J., Jonnalagadda, P., & Savini, G. 2009, Appl. Opt., 48, 3614
- O'Brien, R. C. 2010, PhD thesis, University of California Berkeley
- Page, L., et al. 2007, ApJS, 170, 335
- Pancharatnam, S. 1955, Proceedings Mathematical Sciences, 41, 137, 10.1007/BF03047098
- Planck Collaboration et al. 2011, ArXiv e-prints, 1101.2029
- Polsgrove, D. E. 2009, PhD thesis, University of Minnesota
- Reichborn-Kjennerud, B., et al. 2010, in Presented at the Society of Photo-Optical Instrumentation Engineers (SPIE) Conference, Vol. 7741, Society of Photo-Optical Instrumentation Engineers (SPIE) Conference Series
- Runyan, M. C., et al. 2010, in Society of Photo-Optical Instrumentation Engineers (SPIE) Conference Series, Vol. 7741, Society of Photo-Optical Instrumentation Engineers (SPIE) Conference Series
- Seljak, U., & Zaldarriaga, M. 1997, Physical Review Letters, 78, 2054
- Stivoli, F., Grain, J., Leach, S. M., Tristram, M., Baccigalupi, C., & Stompor, R. 2010, MNRAS, 408, 2319
- Zaldarriaga, M., & Seljak, U. 1998, Phys. Rev. D, 58, 023003